Modelling of impaired cerebral blood flow due to gaseous emboli

Journal Item

Modelling of impaired cerebral blood flow due to gaseous emboli

J.P. Hague [1], C. Banahan [2] and E.M.L. Chung [3,4]

[1] Department of Physical Sciences, The Open University, Walton Hall, Milton Keynes, MK7 6AA, UK

[2] Medical Physics Department, Leicester Royal Infirmary, University Hospitals of Leicester NHS trust, LE1 5WW, UK

[3] Department of Cardiovascular sciences, University of Leicester, Leicester LE1 5WW, UK

[4] Leicester NIHR Biomedical Research Unit in Cardiovascular Disease, Glenfield Hospital, Leicester, LE3 9QP, UK

Abstract. Bubbles introduced to the arterial circulation during invasive medical procedures can have devastating consequences for brain function but their effects are currently difficult to quantify. Here we present a Monte-Carlo simulation investigating the impact of gas bubbles on cerebral blood flow. For the first time, this model includes realistic adhesion forces, bubble deformation, fluid dynamical considerations, and bubble dissolution. This allows investigation of the effects of buoyancy, solubility, and blood pressure on embolus clearance.

Our results illustrate that blockages depend on several factors, including the number and size distribution of incident emboli, dissolution time and blood pressure. We found it essential to model the deformation of bubbles to avoid overestimation of arterial obstruction. Incorporation of buoyancy effects within our model slightly reduced the overall level of obstruction but did not decrease embolus clearance times. We found that higher blood pressures generate lower levels of obstruction and improve embolus clearance. Finally, we demonstrate the effects of gas solubility and discuss potential clinical applications of the model.

1. Introduction

Bubbles entering the cerebral circulation can have devastating consequences for brain function, and are most commonly either created *de novo* during decompression sickness, or inadvertently introduced to the circulation during cardiovascular interventions, particularly open heart surgery featuring cardio-pulmonary bypass. Previous animal studies have shown that a rapid influx of large volumes of air has potential to be fatal [Weenink et al., 2012], and in humans it is speculated that introduction of smaller bubbles could be a potential cause of post-operative neurocognitive decline following cardiac surgery [Barak and Katz, 2005].

Once lodged in the cerebral arteries, bubbles obstruct blood flow causing downstream tissue to be starved of oxygen and pressure changes to be induced in the

surrounding vessels. Since brain tissue is particularly sensitive to a shortage of oxygen (hypoxia), arterial blockages can lead rapidly to irreversible biochemical changes and cell death [Lipton, 1999]. In recent years there has been increasing clinical interest in understanding the relationship between impaired embolus clearance, systemic blood pressure, and cerebral autoregulation [Screiber et al., 2009, Caplan and Hennerici, 1998]. Improved modelling approaches present new possibilities for examining such relationships with a view to guiding strategies to improve patient outcome.

To attempt to quantify the effects of solid and gaseous emboli of varying size, we previously developed a minimal model to forecast the impact of embolisation on blood flow [Chung et al., 2007, Hague and Chung, 2009]. Our previous model featured a very limited description of embolisation, in which emboli were assumed to behave as rigid spheres that block vessels of similar size. The model had a highly simplified description of the fluid dynamics, assuming that all pressure was dropped over the arterioles, and that flow at each bifurcation was governed only by the number of arterioles receiving flow downstream. In this paper, we present a superior model describing motion of deformable gas bubbles through the vasculature, which includes the effects of buoyancy, solubility and blood pressure.

There are a number of differences between solid emboli (which may be almost incompressible and rigid) and gaseous emboli that compress and distort easily [Branger and Eckmann, 1999]. These differences have potential to affect the locations in the vasculature where emboli become lodged and to influence dissolution time. Gaseous emboli have a propensity to deform as they move through the vasculature and only block arteries when the surface area in contact with the walls generates sufficient static friction (stiction) to oppose motion [Suzuki and Eckmann, 2003]. Another significant difference between solid and gaseous emboli is the high buoyancy of gas bubbles, which has potential to influence embolus trajectory. This paper goes beyond previous work by introducing a number of extensions that are needed to properly model the motion of gaseous emboli through the vascular tree: (1) the emboli are deformable (2) an approximation for stiction is included, (3) an iterative fluid dynamical analysis is carried out to estimate the pressure drop in the whole tree, and (4) an estimate of buoyancy effects is included.

The aim of this paper is to provide a model of gas embolisation to help to understand the relationship between fluid dynamical factors, the accumulation of embolic blockages, and impaired bubble clearance for future use in real-time modelling of embolisation. For the first time, we include the effects of blood pressure, embolus buoyancy, bubble deformation, and a realistic parameterisation for the stiction and dissolution of emboli. We begin by introducing our model (section 2). Example results showing the impact of buoyancy, blood pressure and solubility on blockage can be found in section 3. We then consider possible clinical applications in section 4 and provide a summary of our results (section 5).

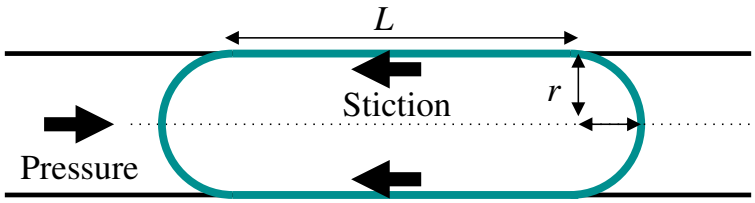

Figure 1. Schematic of a deformable embolus in a vessel, highlighting the mechanisms that lead a gas bubble to block an artery. Blood pressure leads to a force, which is opposed by stiction. When the limiting stiction is larger than the force on the bubble from the blood, the artery becomes blocked.

2. Model

2.1. Bifurcating tree

At bifurcations, the radii of parent and daughter vessels are related by the equation,

$$r_p^\gamma = r_{dA}^\gamma + r_{dB}^\gamma \tag{1}$$

where we set the bifurcation exponent $\gamma = 3$ to be consistent with Murray's law [Murray, 1926a,b] (for information on recent work, see e.g. Fung [1997], Zamir [2000]), r_p is the radius of the parent vessel, and r_{dA} and r_{dB} are the radii of the daughter vessels. We assume a symmetric tree with $r_{dA} = r_{dB} = r_d$, taking the radius of the root node to be 0.5 mm. Therefore, at each level of the tree, $r_d = (2)^{-1/3} r_p$, or in terms of the level, i, of the tree, $r_i = 2^{-i/3} r_0$ where $i = 0$ is the root node of radius r_0. The tree used in the example simulations presented in this paper comprises 18 levels, extending from a trunk radius of 0.5 mm to 9.84 μm arterioles. The number of levels and the diameter of the root node can be adjusted to suit a particular clinical application. In the following, the root node of the tree was assumed to be 1 mm in diameter, as this is similar to the minimum diameter vessel that can be imaged using Magnetic Resonance Angiography (i.e. the topology of larger vessels could be modelled based on imaging data). For ultrasound embolus detection applications the radius of the root node should be adjusted to match the radius of the insonated vessel (typically 2.5 mm for Middle Cerebral Artery insonation [Chung et al., 2006, Banahan et al., 2012]). The model of a bifurcating tree for vessels of less than 1 mm is justified by analysis of high-resolution images of the human cortex [Cassot et al., 2006], which reveal that 94% of branches in the cerebral vasculature consist of bifurcations ‡. Following West, the lengths of the vessels in our model were taken to be proportional to their radii ($l \propto r$) [West et al., 1997].

2.2. Gaseous emboli

Gaseous emboli differ from solid thrombus and plaque since they are deformable and rapidly dissolve. To incorporate the effects of deformability and stiction we assume

‡ Of the remaining nodes, 4% are trifurcations, 1% simple nodes and 0.5% have 4 or more daughters

that a gaseous embolus in a vessel of similar size deforms to a sausage-like shape (shown schematically in figure 1). This shape is a common finding in the cerebral arteries of patients following cardiac surgery, where autopsy reveals large numbers of sausage-like arteriole dilatations [Moody et al., 1990]. The surface area of the embolus touching the side of the vessel is computed by correcting for a domed end with the same radius as the vessel. The length of the cylindrical part of the embolus is $L = (V_{\text{emb}} - 4\pi r_{\text{vessel}}^3/3)/\pi r_{\text{vessel}}^2$, and the surface area touching the side is $2\pi r_{\text{vessel}} L$.

An embolus will come to rest when the pressure drop over a stationary embolus is insufficient to overcome stiction, because the force on the embolus generated by the pressure drop, $\pi r_{\text{vessel}}^2 \Delta p$ is less than the limiting force of stiction, $2K\pi r_{\text{vessel}} L$, i.e. $\pi r_{\text{vessel}}^2 \Delta p < 2K(V_{\text{emb}} - 4\pi r_{\text{vessel}}^3/3)/r_{\text{vessel}}$. The coefficient of stiction has been measured to be $K = 10$ Nm^{-2} [Suzuki and Eckmann, 2003]. The pressure drop for the stationary embolus is equal to the difference between the pressure at the bifurcation upstream from the embolus and the capillary network (since there is no blood-flow in vessels downstream of the embolus the pressure is equal to that of the capillaries).

Based on theoretical considerations, Branger *et al.* (see Eq. 19 in Branger and Eckmann [1999]) previously developed a model parameterisation to describe the time that a gaseous embolus of initial volume V_0 in mm^3 will take to dissolve,

$$T'_X = 2m_X \pi^{1/3} V_0^{2/3} (2 + X)(4/3 + X)^{-2/3} \tag{2}$$

where $X = L/r$ is the aspect ratio of the embolus given by the length of the cylindrical section of the bubble, L, divided by the radius, r, of the artery (see Fig. 1). The parameter m_X impacts directly on the lifetime of the bubble for a specific aspect ratio, X, and has been calculated for two aspect ratios in Branger and Eckmann [1999] to give $m_0 = 97.5$ min/mm^2 for a spherical bubble, and $m_{2.6} = 130.9$ min/mm^2 where the bubble is cylindrical ($X = 2.6$). We can rearrange this relation to calculate the volume of the bubble at time t_{emb} since it was introduced to the model using:

$$V(t_{emb}) = (4/3 + X)\sqrt{\frac{1}{\pi}\left(\frac{T_X - t_{emb}}{m_X(4 + 2X)}\right)^3} \tag{3}$$

where T_X and t_{emb} are in mins. Given the limited information regarding m_X, we assumed the relation for a spherical bubble ($X = 0$) in all subsequent calculations. This represents a best case scenario with fastest dissolve times. These equations describing bubble dissolution have been validated *in-vivo* for small emboli by Branger and Eckmann [1999], and are thought to be scalable to much larger emboli since the underlying equations represent gaseous diffusion over a surface and should be approximately valid for all embolus sizes. When we consider gases other than air, the parameter m_X is scaled accordingly.

2.3. Fluid dynamics and recursive computation

The need to determine the pressures at bifurcations in the arterial tree is an added complication of dealing with deformable gaseous emboli, and means that at least a basic

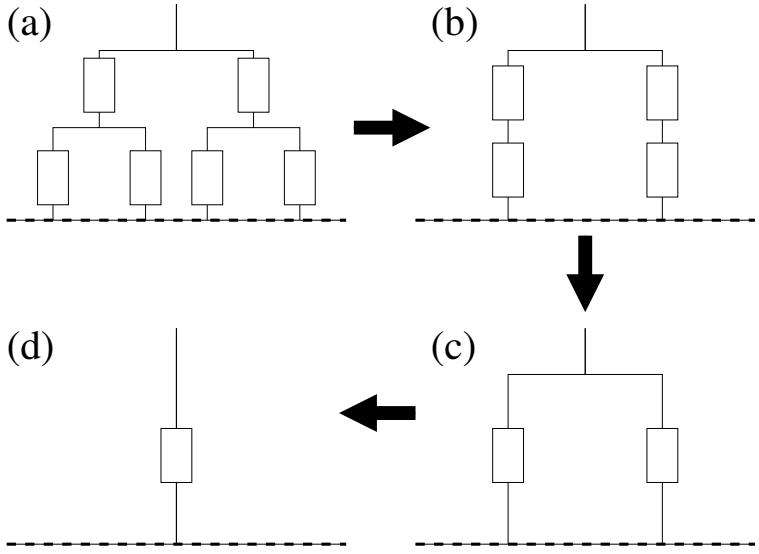

Figure 2. Schematic of the recursive procedure for computing pressures, flows and resistances. Pairs of parallel and serial resistances are rewritten as a single resistance recursively through the whole tree until a single resistance remains. The flow through the single resistor can be calculated, and then the procedure is carried out in reverse, calculating pressures, flows and resistances at each level in the tree.

fluid dynamical analysis of flows in the tree is required. The treatment of pressure in our model also has the important advantage of enabling us to investigate the theoretical impact of blood pressure changes on embolus clearance.

When considering the stiction of gas bubbles, it is essential to determine the pressure difference either side of the embolus. Since pressures need to be computed whenever an embolus moves, and the bifurcating tree in the model has a very large number of nodes, it is essential that a simplified fluid dynamics scheme is used to reduce computation time. We treat the fluid flow through the tree as Poiseuille flow, where the pressure drop across a segment is $\Delta p = Rf$, where f is the flow through the segment and R acts as a resistance, where $R \propto l/r^4$. Since we assume $l \propto r$, $R \propto 1/r^3$, and substituting $r_i = 2^{-i/3} r_0$, the resistance at each level is given by $R_i \propto 2^i$. The pressure drop and effective resistance can be treated using an electrical circuit analogue approach by identifying Δp as a potential difference, and f as a current (see e.g. Murray [1964]). Thus, parallel resistances can be rewritten as a single resistor, and this can be repeated recursively up the tree, working from the end arterioles to the parent node, to compute all flows and pressures as an order N operation, where N is the number of vessels in the tree. This process is summarised in figure 2, and leads to rapid computations which are far faster than using matrix inversion or by directly solving simultaneous equations.

Panel (a) shows the initial bifurcating tree. In panel (b), the smallest vessels have been summarised as a single equivalent resistance. In panel (c) the resistances in series have been simplified, and in panel (d) the recursive step has been applied to the tree that resulted in (c). Clearly, this procedure can be applied to any size of bifurcating tree. Once a single resistance is obtained for the whole tree, the flow into the tree is

calculated, and the recursion is followed backwards, computing pressures and flows at every point (e.g. flows and pressures can be computed at step (b) as there is effectively a potential divider in each branch at that stage. During the recursive procedure, these flows and pressures are stored, and the stored pressures and flows can be used for all calculations until any new blockages are introduced or existing blockages are freed as emboli dissolve.

2.4. Buoyancy

The effects of buoyancy were emulated by introducing a probability weighting, $w_A = (1 + A_g \cos(\theta))/2$, related to the orientation of the branches with respect to gravity. A_g is a parameter that varies between 0 and 1, where $A_g = 0$ represents no correction due to buoyancy (where $w = 1/2$, as in the previous version of the model) and $A_g = 1$ represents an extreme correction. This type of weighting is consistent with the results in Eshpuniyani et al. [2005], where θ is the angle between the plane of the bifurcation and the horizontal. We note that this form for the weighting is *ad-hoc*, but running the code with $A_g = 1$ will demonstrate the essence of the corrections that are required to describe highly buoyant bubbles. Once the additional weighting factors are introduced, the probability that an embolus travels in direction A at a bifurcation is,

$$P_A = w_A f_A / (w_A f_A + w_B f_B) \tag{4}$$

with $P_B = 1 - P_A$, where f_A and f_B designate flows in the A and B directions. θ is assigned randomly to each bifurcation for each instance of the ensemble at time $t = 0$. In future it may be possible to include realistic values for θ for the cerebral arterial tree based on imaging data or models of angiogenesis.

2.5. Algorithm

The algorithm begins by calculating flows, pressures and resistances for an empty tree (using the procedure in section 2.3). It then proceeds as follows:

(i) On any time step, an embolus may be created in the root node of the tree with probability $P_\tau \Delta\tau$ with size randomly chosen between 0 and $r_{\max}$. Here P_τ is the probability per unit time to create an embolus and $\Delta\tau = 1s$ is the length of the time step.

(ii) All emboli dissolve leading to a reduction in radius during each time step according to the parameterisation in Sec. 2.2. Completely dissolved emboli are removed from the simulation. If the reduction in radius generates a change in the blockage state of the tree, flows and pressures are recalculated.

(iii) The emboli move according to the following rules:

  (a) If the pressure behind the deformed embolus is insufficient to overcome stiction it does not move. (See section 2.3)

  (b) If all arterioles downstream are blocked, the embolus may not move since there is no flow.

(c) If the embolus radius becomes smaller than the current node and there is flow downstream:
   1. The flows in directions A and B are determined by solving our simplified fluid dynamics scheme.
   2. The embolus then moves in direction A with probability $P_A = f_A w_A/(f_A w_A + f_B w_B)$. Otherwise, it moves in direction B.

(iv) If progress of an embolus generates a new blockage, then the pressures and flows are recalculated. At this stage numerical measurements of the state of the tree are repeated.

2.6. Bubble deformation

To confirm the importance of accounting for bubble deformation within the model the percentage of blocked end arterioles was estimated for hypothetical non-deformable bubbles that were assumed to remain spherical and become lodged when encountering vessels of equal diameter. When bubbles were not assumed to deform the proportion of blocked nodes rapidly increased to 100% and the instantaneous percentage of blocked end arteries was significantly overestimated. Example simulations featuring deformable and hypothetical non-deformable bubbles are shown in figure 3.

3. Results

Since the model is highly flexible and includes a large number of parameters, the next few sections provide example simulations illustrating the effects of buoyancy, blood pressure, and solubility with all other parameters held fixed. In the absence of clinical data, showers of simulated emboli were generated using a random number generator, which selected embolus radii from a flat distribution ranging from 0 to $r_{\max}$ (the average embolus radius being $r_{\max}/2$). For all simulations, embolisation was assumed to commence at $t = 10$ s. Emboli were introduced to the tree at randomly generated times centred on a mean embolisation rate of 1 embolus/second until the total number of emboli to be simulated had been delivered. In each simulation the size range of incoming emboli, solubility, buoyancy, blood pressure, and the total number of emboli were varied. To simulate bubbles, all emboli were assumed to be deformable and highly buoyant ($A_g = 1$). The average statistical behaviour of the system was determined from an ensemble of 100 simulations. Outputs of the model include (i) the instantaneous number of end arterioles receiving no flow, (ii) the number of end arterioles without flow for a particular duration (10 mins, 1 hr, or 2 hrs.), and (iii) total time required for washout. Benchmarks of 10 minutes, 1 hr and 2 hrs for obstruction of individual arterioles were chosen to reflect clinically relevant time-scales over which it is thought that neuronal changes might occur.

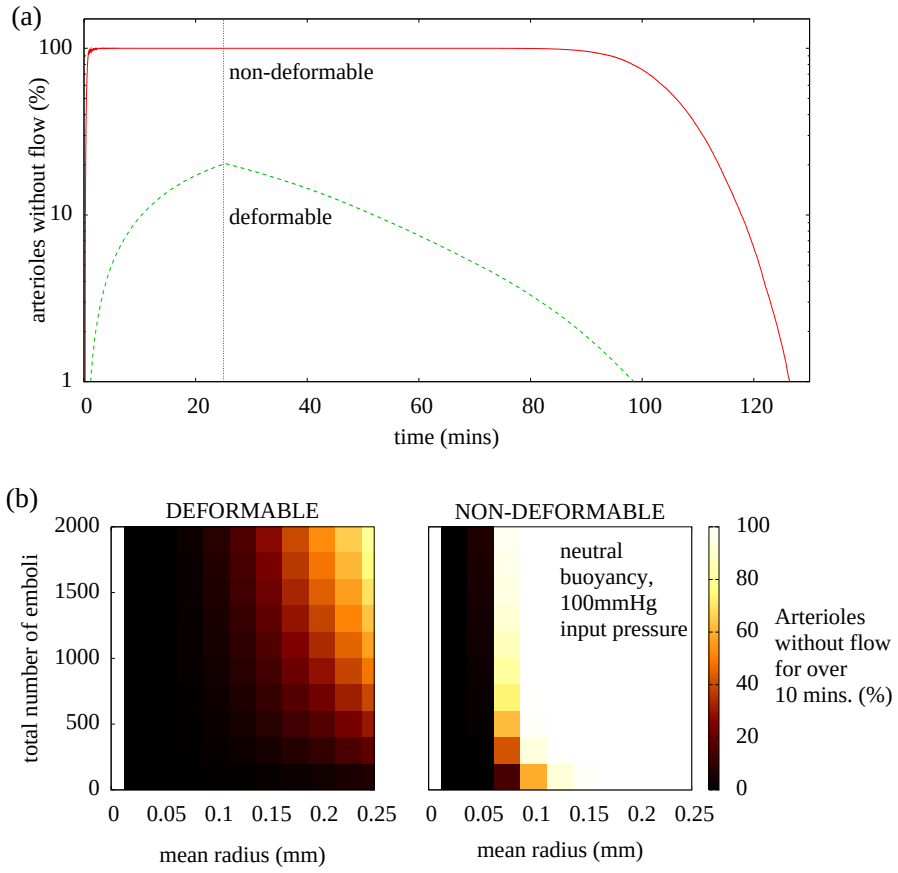

Figure 3. Example simulations comparing the instantaneous percentage of end arteries receiving no flow vs time for hypothetical non-deformable bubbles that remain spherical as they enter the tree compared to more realistic bubbles that deform to the diameter of the vessel. [$P = 100mmHg$, $A_g = 0$, embolisation rate = 1 emb/s]. (a) When the bubbles are assumed to be spherical and non-deformable the total number of blocked end arterioles rises rapidly and the vascular tree quickly bcomes fully blocked (solid line). Deformation of the bubbles as they enter narrow vessels generates an order of magnitude reduction in the proportion of arterioles without flow (dashed line). The vertical dotted line indicates the time at which embolisation ceases. The total time required for non-deformable bubbles to wash out of the system was longer than for deformable bubbles [$n = 1500$, $r_{max} = 0.3$ mm]. Panel (b) shows the proportion of end nodes receiving no blood supply for over 10 mins, plotted as a function of total number of emboli (y-axis) and average embolus radius (x-axis), for deformable and non-deformable emboli. If no blockage is registered, then the cell is black. For non-deformable bubbles larger than approximately 0.1 mm average radius the tree was fully blocked. These results confirm that it is essential to include embolus deformation in the model to avoid overestimation of the proportion of blocked nodes.

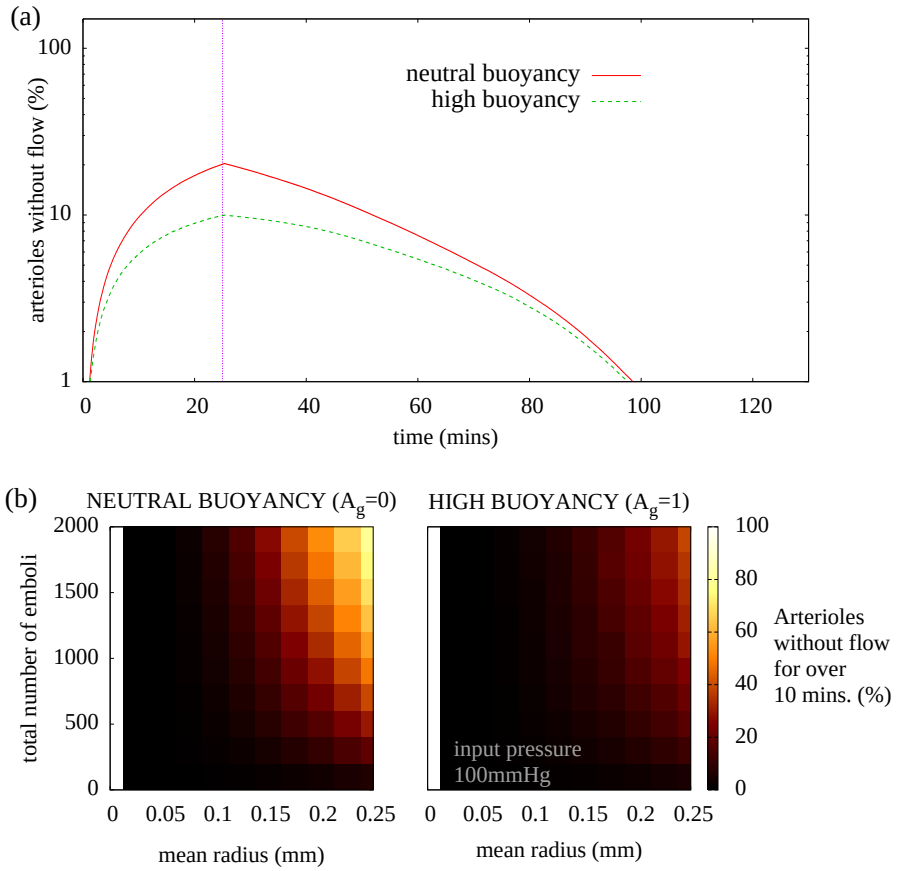

Figure 4. (a) Example simulations comparing the instantaneous percentage of end arteries receiving no flow vs time for neutrally buoyant($A_g = 0$) and highly buoyant ($A_g = 1$) bubbles. [P = 100mm Hg, mean embolisation rate = 1 emb/s] (a) After embolisation begins, embolic blockages accumulate and tend toward a dynamic equilibrium level (where similar numbers of emboli are dissolving and leaving the model vasculature as entering). Buoyancy reduces the proportion of end arterioles without flow because certain paths through the tree become more probable when emboli are buoyant. In the washout phase, emboli dissolve without being replaced and the percentage of end arteries experiencing impaired blood flow gradually returns to zero. However, the total time taken for embolus clearance is not reduced by the effects of buoyancy, which indicates regional intensification. [$n = 1500$, $r_{\max} = 0.3$ mm] (b) shows 2D plots illustrating the effects of buoyancy on the number of individual end arterioles that received no flow for over 10 mins as a function of total number of emboli and average radius.

3.1. Buoyancy

Example simulations presented in figure 4 illustrate the effects of buoyancy on the number of end arterioles receiving no flow and time required for embolic washout. In panel (a) emboli are randomly generated with an average radius of $r_{\text{av}} = 0.15$ mm (randomly selected from a flat distribution from 0 to $r_{\max}$=0.3 mm). The period of embolisation features 1500 emboli introduced at an average rate of one embolus every

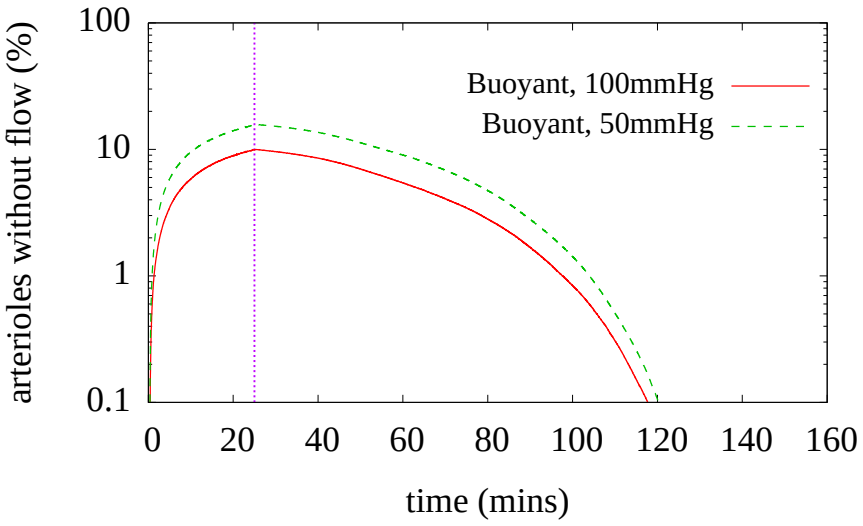

Figure 5. Instantaneous blockages for input pressures of 50 and 100 mm Hg with all other parameters held constant. [$A_g = 1$, $n = 1500$, $r_{\max} = 0.3$ mm, embolisation rate = 1 emb/s]

second over a period of approximately 25 mins. For reference, an average 0.15 mm radius bubble in this simulation is estimated to take 27.6 minutes to dissolve while the largest 0.30 mm radius bubble takes 110 minutes. As in our previously published model, after embolisation begins the proportion of end arterioles without flow tends toward a dynamic equilibrium level [Chung et al., 2007]. However, here we are also interested in embolus clearance, so we allow embolisation to cease and emboli to wash out. Following embolisation, existing emboli dissolve and blockages are cleared.

The effects of buoyancy can be seen to slightly reduce the proportion of blocked end arterioles due to some paths through the tree becoming more probable than others. This decreases the total number of obstructed end arterioles but was not found to reduce the time for embolic washout. This effect is expected to be especially pronounced for highly buoyant emboli ($A_g = 1$) since buoyancy leads to preferred paths through the vasculature and a higher probability of emboli obstructing the same nodes.

3.2. Blood pressure

To demonstrate the impact of blood pressure changes on the total number of end arterioles without flow, simulations were performed for input pressures of 50 and 100 mmHg. The total instantaneous percentage of end arteries receiving no flow decreases with increasing pressure, see figure 5.

Figure 6 shows the effects of doubling the input pressure on the percentage of end arterioles that were obstructed for longer than 10 minutes, 1 hour and 2 hours. In all simulations, bubbles were assumed to be deformable and highly buoyant. These results suggest that the duration of embolic blockages due to gas emboli can be expected to fluctuate with changes in blood pressure. We find that increased blood pressure leads

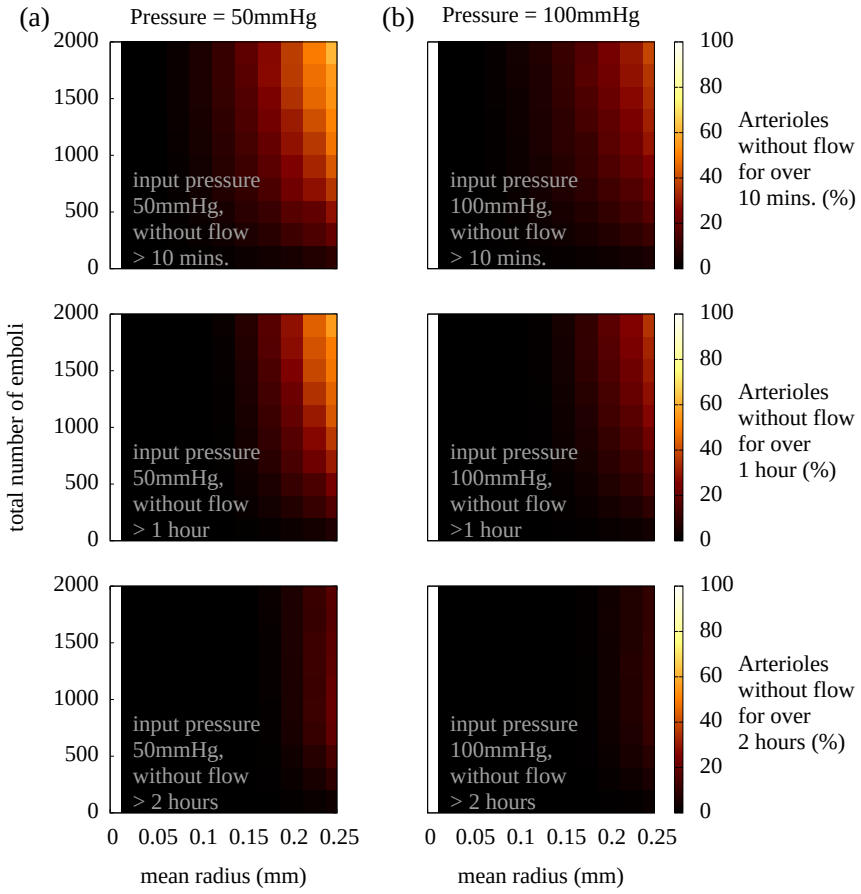

Figure 6. The proportion of end arterioles receiving no supply for 10 minutes, 1 hour, and 2 hours for buoyant emboli of varying number (y-axis) and size (x-axis). The pressure at the root node is 50 mmHg in the l.h.s. panels and 100 mmHg on the r.h.s. Emboli were introduced at a rate of 1 emb/s and $A_g = 1$.

to a reduction in both the total number and duration of embolic blockages.

3.3. Solubility

Finally, we investigated the effects of altering the dissolve rate of emboli, figure 7. Although the simulations performed as part of this study are purely hypothetical, in practice a faster dissolve rate could be achieved by replacing air with a more soluble gas such as CO_2. Increasing the dissolve rate of emboli by a factor of 20 was found to significantly reduce the duration of blockages. Figure 7(a) shows the instantaneous percentage of arterioles receiving no flow for 1500 emboli incident on the tree at an average rate of 1 embolus per second, with an average radius of 0.15 mm (0.3 mm maximum radius). The increase in dissolve rate significantly decreased the total number of blocked end arteries and was observed to have a striking impact on the total time taken for emboli to wash out of the system. Panel (b) shows the reduction in arterioles receiving no flow for over 10 minutes.

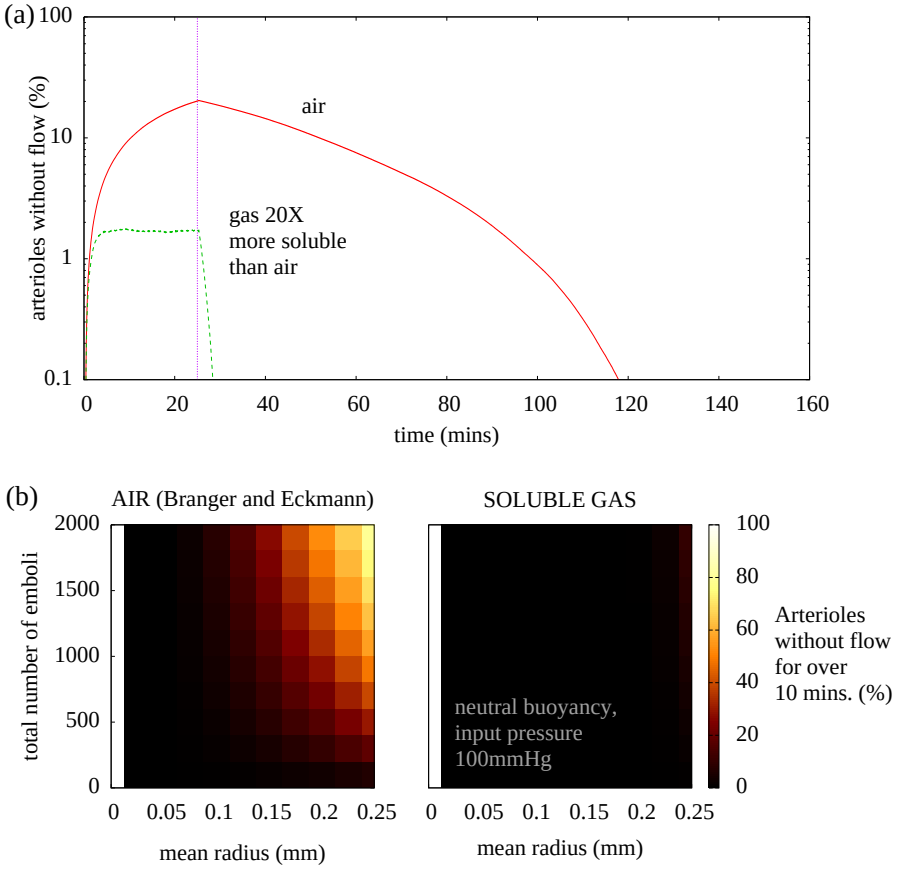

Figure 7. (a) Example simulations showing the accumulation of embolic blockages and washout phase for air compared to a gas that is 20 times more soluble. Increased solubility reduces the instantaneous percentage of arterioles receiving no flow and blockages clear almost instantaneously once embolisation ceases. [P = 100 mmHg, $A_g = 1$, $n = 1500$, $r_{\max} = 0.3$ mm, embolisation rate = 1 emb/s] (b) Percentage of model terminal arterioles without flow for at least 10 minutes for air compared to a gas that is 20 times more soluble. The increase in dissolve rate leads to a dramatic reduction in blockage. Even for simulations featuring bubbles with radii approaching that of the root node (0.5 mm max radius) virtually no end arterioles remained obstructed for longer than 10 minutes. [$P = 100$ mmHg, $A_g = 1$, embolisation rate = 1 emb/s]

4. Discussion

Despite air embolism representing an important clinical problem, surprisingly little theoretical modelling has previously been undertaken to try to quantify the impact of bubbles on cerebral blood flow. The current study contributes to our understanding of the accumulation of emboli, interplay between blood pressure and bubble properties, and the process of embolic washout. To the best of our knowledge, our model is the first to incorporate realistic bubble deformation, solubility, buoyancy, and stiction.

Figure 3 illustrates the importance of modelling bubble deformation. In the absence

of deformation the total instantaneous percentage of arterioles without flow rises rapidly and is significantly overestimated. Assuming hypothetical non-deformable spherical bubbles the arterial tree quickly reaches saturation.

In the results section we presented results for deformable emboli and investigated the effects of buoyancy, blood pressure and solubility. The effects of buoyancy of the bubbles can be seen in figure 4 to slightly reduce the total number of end arteries receiving no flow without decreasing the total time required for emboli to completely wash out of the tree.

An interesting finding of our model was the relationship between embolisation dynamics, washout of bubbles, and blood pressure. An increase in blood pressure was found to decrease the proportion of blocked arterioles (figures 5 and 6) and appeared to slightly reduced the time required for bubbles to clear. Our results suggest that an increase in blood pressure may assist in forcing bubbles through the vascular tree more rapidly, thereby reducing the total number of affected arterioles. This is based on the principle that higher pressures push gaseous emboli further into the tree, which reduces the total area of the vasculature that will be affected, (since the number of nodes downstream from a blockage halves at each bifurcation). A similar effect would also be expected to be associated with a decrease in stiction through the introduction of surfactants. This method for reducing the impact of air emboli has previously been tested in animals but not in humans [Barak and Katz, 2005]. We note that a change in blood pressure will slightly modify the solubility here [Branger and Eckmann, 1999] (for example change in blood pressure from 100mmHg to 50mmHg will decrease the total pressure in the blood - the sum of atmospheric pressure and blood pressure - by approximately 5%, leading to similar proportional changes in the dissolve rate).

Gas solubility had an impact on both the instantaneous number of arterioles without flow and bubble clearance time; more rapid dissolve times led to faster embolus clearance, figure 7. The dramatic reduction in the total number of end arterioles receiving no flow suggests that if bubbles were formed from a much more soluble gas (such as CO_2) both the percentage of arterioles without flow and clearance time would dramatically reduce. At the faster dissolve rate no arterioles experienced blockages lasting longer than 20 mins and the washout period was negligible. This finding is consistent with *in vivo* research conducted on animals showing that the fatal dose of injected arterial gas is around 50 times higher for infusion with CO_2 than for air [Moore and Braselton, 1940]. Our results are also consistent with ultrasound embolus detection studies during cardiac surgery which show that flooding of the operative area with CO_2 reduces the number of emboli detected in the cerebral bloodstream by 75% [Svenarud et al., 2004]. It is hoped that combining our simulations with clinical detection and sizing of bubbles,[Banahan et al., 2012], will enable us to help answer some of these ongoing research questions in future work.

As the model remains highly simplified it retains a number of limitations. Firstly, our tree is completely symmetric and bifurcation angles were randomly assigned at the start of each simulation. We are currently in the process of growing anatomically

realistic cerebral vasculatures *in-silico* and hope to have an opportunity to combine these with patient specific clinical imaging data, computational forecasting, and multi-scale modelling of diffusion and biochemical interactions in future work. In our model, gaseous emboli do not split at bifurcations or coalesce. Bubble splitting is likely to affect embolus trajectory at bifurcations angled within, or close to, the horizontal plane. In our model of bubble dissolution, we do not include a treatment of the change in dissolution time due to bubble deformation. Also, we assume that the forces required to lodge and dislodge the bubble are equal. So far, we have only considered steady flow conditions (e.g. during cardiopulmonary bypass), however, we expect to be able to include windkessel equations to also describe pulsatile flow in future models. In view of these limitations, the results of the current study are not intended to inform clinical practice, but rather, may highlight areas of interest for further study.

Although the total instantaneous percentage of end arteries without flow is of limited clinical value, we also investigated the proportion of arterioles that theoretically received zero flow for longer than a pre-defined cut-off time (e.g. 10 mins, 1 hr, 2 hrs). Further work is required to relate the duration of impaired perfusion to models of cell death describing the timescale of neuronal changes, reversible ischaemia, and irreversible tissue damage [Lipton, 1999]. This is likely to require the development of multi-scale models of cell death, which combine cellular biochemical interactions, solution of localised diffusion equations, and realistic embedding of the vasculature within brain tissue. Further work will also be required to incorporate the impact of haemodilution (which is highly relevant in a cardiac surgery setting), collateral flow, and cerebral autoregulation.

By combining a realistic description of the deformation and dissolution of bubbles with a symmetric model of the cerebral arterial tree and a simplified description of fluid dynamics, we believe that we have succeeded in qualitatively understanding the likely extent and duration of cerebral embolic blockages due to gas bubbles. Given recent advances in bubble sizing [Banahan et al., 2012], and knowledge of patient-specific anatomy and physiology, we anticipate that it will soon be possible to make intra-operative predictions of the impact of embolisation during surgery.

5. Summary

This paper describes a Monte-Carlo simulation used to model the motion of gaseous emboli through the cerebral vasculature. Our model improves on previous research by modelling deformable gas bubbles and includes realistic stiction effects, fluid dynamical considerations (including blood pressure), and a basic description of embolus buoyancy. We show that our model can be used to investigate the dynamic nature of cerebral embolisation and to estimate the duration of impaired blood flow in individual arterioles over time. Using this model it becomes possible to examine the effects of input pressure, embolus composition, buoyancy, stiction, size, and embolisation rate on cerebral blood flow. We found that deformation of gas bubbles is crucial for quantifying embolic

obstruction in response to blood pressure. We also give examples of the potential of our model for investigating factors that influence the impact of gaseous emboli during surgery. Buoyancy effects tend to influence embolus trajectory and generate regional intensification of blockages. Since the accumulation of embolic blockages is partly dependent on blood pressure, maintenance of higher blood pressures might improve embolic washout by rapidly forcing bubbles through the vasculature, and may be worth further study. We also confirm that replacement of air with a more soluble gas could theoretically eliminate the risk of gas embolism.

Acknowledgments

EMLC is a British Heart Foundation Intermediate Basic Science Research Fellow (FS/10/46/28350). CB and EMLC acknowedge support for this study from the Leicestershire, Northamptonshire and Rutland Comprehensive Local Research Network (CLRN). This study is part of the research portfolio supported by the Leicester NIHR Biomedical Research Unit in Cardiovascular Disease. We acknowledge useful discussions with Jonathan Keelan and David Marshall.

References

C. Banahan, J.P. Hague, D.H. Evans, R. Patel, K.V. Ramnarine, and E.M.L.Chung. Sizing gaseous emboli using doppler embolic signal intensity. *Ultrasound in Med. and Biol.*, 38:824, 2012.

M. Barak and Y. Katz. Microbubbles: Pathophysiology and clinical implications. *Chest*, 128:2918–2932, 2005.

A.B. Branger and D.M. Eckmann. Theoretical and experimental intravascular gas embolism absorption dynamics. *J. Appl. Physiol.*, 87:1287–1295, 1999.

L.R. Caplan and M. Hennerici. Impaired clearance of emboli (washout) is an important link between hypoperfusion, embolism, and ischemic stroke. *Arch. Neurol.*, 55:1475–1482, 1998.

F. Cassot, F. Lauwers, C. Fouard, S. Prohaska, and V. Lauwers-Cances. A novel three-dimensional computer-assisted method for a quantitative study of microvascular networks of the human cerebral cortex. *Microcirculation*, 13:1–18, 2006.

E.M.L. Chung, L. Fan, A.R. Naylor, and D.H. Evans. Characteristics of doppler embolic signals observed following carotid endarterectomy. *Ultrasound Med. Biol.*, 32:1011–1023, 2006.

E.M.L. Chung, J.P. Hague, and D.H. Evans. Revealing the mechanisms underlying embolic stroke using computational modelling. *Phys. Med. Biol.*, 52:7153–7166, 2007.

B. Eshpuniyani, J. B. Fowlkes, and J.L. Bull. A bench top experimental model of bubble transport in multiple arteriole bifurcations. *Int. J. Heat Fluid Flow*, 26:865, 2005.

Y.C. Fung. *Biomechanics: Circulation*. Springer-Verlag, New York, 1997.

J.P. Hague and E.M.L. Chung. Statistical physics of cerebral embolization leading to stroke. *Phys. Rev. E*, 80:051912, 2009.

P. Lipton. Ischemic cell death in brain neurons. *Physiological Review*, 79:1431–1568, 1999.

D.M. Moody, M.E. Bell, V.R. Challa, W.E. Johnston, and D.S. Prough. Brain microemboli during cardiac surgery or aortography. *Ann. Neurol.*, 28:477–486, 1990.

R.M. Moore and C.W. Braselton. Injections of air and carbon dioxide into a pulmonary vein. *Ann. Surg.*, 112:212–218, 1940.

C.D. Murray. The physiological principle of minimum work applied to the angle of branching arteries. *Journal of General Physiology*, 9:835–841, 1926a.

C.D. Murray. The physiological principle of minimum work. i. the vascular system and cost of blood volume. *Proceedings of the National Academy of Sciences*, 12:207–214, 1926b.

K. Murray. Dimensions of the circle of willis and dynamic studies using electrical analogy. *J. Neurosurg.*, 21:26–34, 1964.

S. Screiber, M. Serdaroglu, F. Schreiber, M. Skalej, H.-J. Heinze, and M. Goertler. Simultaneous occurrence and interaction of hypoperfusion and embolism in a patient with severe middle cerebral artery stenosis. *Stroke*, 40:e478–e480, 2009.

A. Suzuki and D.M. Eckmann. Embolism bubble adhesion force in excised perfused microvessels. *Anesthesiology*, 99:400, 2003.

P. Svenarud, M. Persson, and J. van der Linden. Effect of CO_2 insuflation on the number and behavior of air microemboli in open heart surgery. *Circulation*, 109:1127–1132, 2004.

R.P. Weenink, M.W. Hollmann, and R.A. van Hulst. Animal models of cerebral arterial gas embolism. *Journal of Neuroscience Methods*, 205:233–245, 2012.

G.B. West, J.H. Brown, and B.J. Enquist. A general model for the origin of allometric scaling laws in biology. *Science*, 276:122, 1997.

M. Zamir. *The physics of pulsatile flow*. Springer-Verlag, New York, 2000.